

The initiation temperatures in nanothermite reactions

V.G. Myagkov

Kirensky Institute of Physics, Federal Research Center KSC SB RAS, 660036

Krasnoyarsk, Russia

ORCID 0000-0002-3276-0309

E-mail: miagkov@iph.krasn.ru

Abstract

An assumption on general regularities and chemical mechanisms of solid-state reactions in nanofilms and nanothermite mixtures is made. It is demonstrated that the moving force of all Al-based nanothermite reactions is the synthesis of the Al_2O_3 phase with a high negative enthalpy of formation. According to this assumption, all Al-based nanothermite reactions should have the same initiation temperature T_{in} . Indeed, an analysis of literature data shows that the synthesis of the Al_2O_3 phase in Al/ Fe_2O_3 , Al/ CuO , Al/ Co_3O_4 , Al/ MoO_3 , Al/ Bi_2O_3 , and Al/ NiO nanothermite mixtures starts at the same temperature $T_{\text{in}} \sim 510^\circ\text{C}$. We also demonstrate the same initiation temperatures $\sim 250^\circ\text{C}$, $\sim 300^\circ\text{C}$, and $\sim 180^\circ\text{C}$ for Zr-, Mg- and In-based nanothermite reactions, respectively. It is predicted that nanothermite reactions based on other fuels have their own initiation temperatures.

Keywords: Solid-state reactions, Nanofilms, Nanothermite reactions, First phase, Initiation temperature.

1. Introduction

The control and predictability of the synthesis of new materials is one of the most fundamental challenges in material science. The traditional approach to this problem is to use the prediction of crystal structure from first principles [1- 4]. However, now the lack of control and predictability are indeed notorious characteristics of the synthesis of new materials [5]. The prediction of the phases in binary systems that will be formed during the thin film solid-state reaction has been a subject of numerous studies, and different empirical rules have been developed for predicting first phase formation [6-14].

Studies of solid-state reactions in nanolayers have shown three fundamental features that strongly distinguish them from bulk powders:

(i) Formation of only the first phase at the film reagent interface at a certain temperature T_{in} called the initiation (formation) temperature T_{in} . As the annealing temperature is increased, other phases can occur and form the phase sequence [11-14].

(ii) The threshold of the reaction, characterized by intense intermixing at the interface and formation of compounds, arises at temperatures above the initiation (formation) temperature T_{in} . The values of T_{in} in the first phase can be about room temperature [15, 16] or even at cryogenic temperatures [17-20]

(iii) Migration of the dominant diffusing species through the interface during first phase formation [13, 21, 22].

The formation of only the first phase among equilibrium phases, low initiation temperatures, and migration of the dominant diffusing species are unique, unexplained features of solid-state reactions in nanofilms. From the above results it follows that the first phase and its initiation temperature T_{in} are control characteristics of the thin film solid-state reactions.

2. Presentation of the hypothesis

Over the past decade, investigations focused on the nanoenergetic materials, such as reactive multilayer thin films [23, 24] and nanostructured reactive mixtures [25-27]. Thermite mixtures belong to a wide class of energetic materials that comprise a metal fuel (e.g., Al, Mg, or B) and an oxidizer (e.g., Fe_2O_3 , MoO_3 , CuO , Bi_2O_3 , or WO_3). These mixtures react with a lot of heat release; therefore, the thermite reactions often occur in a self-sustaining mode [28-30]. Typical thermite mixtures contain micron particles and have a combustion wave velocity of 1-20 m/s. In recent years, there has been an increasing interest in nanothermites (superthermites) where the particle size is reduced to a few nanometers. In nanothermite mixtures, the combustion wave velocity grows to 1000 m/s [25-27]. Studies of nanothermite combustion are mainly aimed at measuring the combustion wave velocity, burning temperature, delay time, and their dependences on density, morphology, and composition of the reaction mixture. Despite the intense investigations of thermite reactions, their general regularities and mechanisms remain unclear. Currently, the classical nanothermite Goldschmidt reaction $Fe_2O_3 + 2Al = Al_2O_3 + 2Fe$ and other Al-based reactions are well studied.

In this work, we extend the existing concepts of the first phase and its initiation temperature T_{in} , which describe the initial stage of solid-state reactions in nanofilms onto thermite reactions and demonstrate that in all Al-based nanothermite mixtures the synthesis of the Al_2O_3 phase starts at the same initiation temperature $T_{in} \sim 510^\circ C$. These results open up a way for understanding the exclusive role of the initiation temperature T_{in} in the solid-state

reactions at the nanoscale. Our previous studies and the analysis of solid-state thin film reactions for many bilayers have shown that the initiation temperatures T_{in} often coincide with temperatures T_K of structural phase transformations ($T_{in} = T_K$). In particular, initiation temperatures $T_{in}(\text{Cu/Au})$ and $T_{in}(\text{Ni/Fe})$ of reactions in the Cu/Au and Ni/Fe bilayers coincide with the minimum temperature of the order-disorder phase transition in Cu-Au [31] and the eutectoid decomposition temperature in the Fe-Ni system [32], respectively. In Ni/Al and Cd/Au films, the reactions start at the temperature of the inverse martensitic transformation in the Ni-Al [33] and Cd-Au [34] binary systems, respectively. The equality $T_{in} = T_K$ was also established for the eutectic reactions, superionic transition, and spinodal decomposition in Al/Ge [35], Se/Cu [36], and Mn/Ge [37, 38] films, respectively. The equality $T_{in} = T_K$ indicates the common nature of chemical interactions that control both solid-state reactions in thin films and solid-state transformations.

3. Testing of the hypothesis

The above results demonstrate that the first phase and its temperature T_{in} are the fundamental characteristics of a reaction bilayer. It follows that low-temperature reactions occur only between the reacting layers whose reaction products have low-temperature solid-state transformations. Therefore, the study of phase sequences in reaction couples makes it possible to refine and supplement the phase equilibrium diagrams especially in low-temperature part. Thus, recently we investigated the reaction in Ge/Mn bilayers and confirmed the existence of spinodal decomposition in an in Ge-Mn system at 120°C. It is important to note that the formation of the first Mn_5Ge_3 phase was independent of whether Mn and Ge atoms are in a solid solution or in Ge/Mn bilayers [37, 38].

The one important characteristic of reactive multilayer films is the ignition temperature T_{ig} , which can be defined as a minimum temperature of onset of a self-sustaining reaction for a given experiment [23, 24]. As known, the self-sustaining regime of reaction arises when the rate of heat generation $Q_{reaction}$ overcomes the rate of heat losses Q_{loss} ($Q_{reaction} > Q_{loss}$). Unlike T_{ig} , the initiation temperature T_{in} is the start temperature of reactions at which the rate of heat generation $Q_{reaction}$ is less than the rate of heat losses Q_{loss} ($Q_{reaction} < Q_{loss}$) and so the initiation temperature T_{in} is always less than the ignition temperature T_{ig} ($T_{in} < T_{ig}$). As discussed above the initiation temperature T_{in} is the threshold temperature: no reaction below T_{in} and reaction initiate just the temperature of sample overcomes T_{in} . Thus, the initiation temperature T_{in} is the characteristic temperature of our given reaction couple. In contrast to T_{in} , the ignition temperature T_{ig} is a kinetic quantity that depends on the heating rate and the rate of heat loss. Nevertheless, Frits et

al. have recently shown that, similar to T_{in} , the ignition temperature T_{ig} in Ni/Al multilayers with a given bilayer thickness is a threshold temperature because in hot plate experiments the multilayers do not ignite when the specimens are heated to temperatures just 1°C below T_{ig} [39].

The enthalpy of formation of the first phase is a good measure of the free energy variation during the solid-state interaction; therefore, the heats of formation were used in several initial models to predict the first phase and phase sequence formation. Pretorius *et al.* [13] proposed an effective model for the enthalpy of formation, which was successfully used for predicting the first phase formation in many binary systems.

As mentioned above, with the increasing of the temperature of the bilayer above T_{in} leads to the beginning of intermixing of the reagents and first phase synthesis on the interface and consequently physical characteristics of the film samples, such as electrical resistance, magnetization, transparency, and heat release, begin to radically change. Obviously, the start temperature of these changes is the reaction initiation temperature T_{in} . In most cases the energetic properties of thermite nanocomposites were investigated by differential thermal analysis (DTA), thermogravimetric analysis (TGA), and differential scanning calorimetry (DSC). In this case the initiation temperature T_{in} is the temperature at which heat release starts. An important characteristic of the DSC curves is also the exothermic peak temperature, which, unlike the initiation temperature T_{in} , depends on the heat removal conditions from the reaction zone.

It is important to note that the contaminants that form on the reagent interface during various methods of sample preparation (especially for chemically produced samples) can form thin barrier layers that slightly change the initiation temperature of T_{in} but do not suppress the reaction. An error in finding the exact value of the initiation temperature T_{in} can also follow from the certain inaccuracy in determining T_{in} from DTA, TGA and DSC plots. To find the exact T_{in} value, low heating rates are required. Therefore, we referred only to the studies in which the heat release curves were obtained at minimum heating rates (5,10 or 20 °C/min).

The main results of the work are summarized in the schematic diagram in Figure 1, showing the initiation temperature $T_{in} \sim 510^\circ\text{C}$ of the Al_2O_3 phase in Al/ Fe_2O_3 , Al/ Co_3O_4 , Al/NiO, Al/ MnO_2 , Al/ Bi_2O_3 , Al/CuO, Al/ MoO_3 nanothermite reactions and oxidation of Al nanomaterials.

3. Implication of the hypothesis

3.1. The initiation temperature $T_{in} \sim 510^\circ\text{C}$ of the Al-based nanothermite reactions

It can be seen from Tables 1 – 4 that, taking into account the errors in measuring the DTA, TGA, DSC curves, and magnetic and resistivity plots by different authors, the initiation temperatures of all Al-based nanothermite reactions are centered around ~ 510 °C. As can be seen from Tables 1- 4, at heating rates 5, 10, 20 °C/min the heat release curves also have closely exothermic peak temperatures. It must be noted that at a heating rate of 5 °C/min, the oxidation of nanosized aluminum powders also starts at about 510 °C [60, 92-100]. Recently it was shown that the DSC curves of the NiCo₂O₄/Al core-shell nanowires thermite film [101] and three-dimensional ordered macroporous NiFe₂O₄/Al nanothermites [102] have an exothermic peak with an initiation temperature ~ 530 °C and an exothermic peak temperature ~ 600 °C. This unambiguously proves, that the synthesis of Al₂O₃ is the driving force of the thermite reaction $8\text{Al} + 3\text{Ni}(\text{Co or Fe})_2\text{O}_4 \rightarrow 4\text{Al}_2\text{O}_3 + 3\text{Ni} + 6(\text{Co or Fe})$ in the NiCo₂O₄/Al and NiFe₂O₄/Al nanocomposites.

These results suggest the following reaction mechanism: below the initiation temperature $T_{\text{in}} < \sim 510$ °C, Al and O atoms remain chemically neutral. At $T_{\text{in}} > \sim 510$ °C, strong chemical interactions occur between Al and O atoms that break old chemical bonds causing the directed atomic migration to the reaction zone and the synthesis of Al₂O₃ regardless of the system they exist in. Therefore, the initiation temperature $T_{\text{in}} \sim 510$ °C is a universal parameter of all Al-based nanothermite reactions.

3.2. The initiation temperature $T_{\text{in}} \sim 250$ °C of the Zr-based nanothermite reactions

The driving force of the Zr-based nanothermite reactions is the formation of the ZrO₂ phase, which has a relatively high negative enthalpy of formation ($\Delta H_f = -601$ kJ/mol). The analysis of the synthesis of Co-ZrO₂ and Fe- ZrO₂ ferromagnetic nanocomposites show, that thermite reactions in the Zr/Co₃O₄ [103] and Zr/Fe₂O₃ [104] thin films have the same initiation temperature $T_{\text{in}}(\text{Zr/Co}_3\text{O}_4) = T_{\text{in}}(\text{Zr/Fe}_2\text{O}_3) \sim 250$ °C. This value $T_{\text{in}} \sim 250$ °C is in agreement with the initiation temperature $T_{\text{in}}(\text{Zr/CuO}) \sim 250$ °C in the Zr/CuO nanothermite mixture [105] and with the study where the ZrO₂ nanoparticles were obtained by glycothermal processing [106]. From these facts we predict the same initiation temperature $T_{\text{in}} \sim 250$ °C for all the Zr-based nanothermite reactions.

3.3. The initiation temperature $T_{\text{in}} \sim 450$ °C of the Mg-based nanothermite reactions

The driving force of the Mg-based nanothermite reactions is the synthesis MgO phase having a high negative enthalpy of formation ($\Delta H_f = -1097$ kJ/mol) with some low enthalpy of

formation of Al_2O_3 ($\Delta H_f = -1676$ kJ/mol). Using the results of this paper [105], we determined that the thermite multilayer Mg/CuO stacks the initiation temperature $T_{\text{in}}(\text{Mg/CuO}) \sim 450$ °C. The nearest value of the initiation temperature has nanoenergetic Mg/CuO core/shell arrays, which exhibit an onset reaction temperature (~ 450 °C) [107]. The initiation temperatures are close to ~ 450 °C in fresh CuO/Mg/fluorocarbon nanoenergetic composites [108] and μm -Mg/nmCuO thermite mixtures prepared by physical and ultrasonic mixing [109]. Magnesium particles with a nominal size of 6 μm begin an intensive oxidation above 500 °C, which suggests that the starting temperature of the oxidation of nanosized magnesium powders is below 500 °C [110]. In these papers the initiation temperature T_{in} was defined as the temperature at which heat release started using the curves of differential thermal analysis (DTA), thermogravimetric analysis (TGA), and differential scanning calorimetry (DSC). Although the exact value of the initiation temperature of Mg-based nanothermite reactions remains unknown, it lies around 450 °C.

3.4. The initiation temperature $T_{\text{in}} \sim 180$ °C of the In-based nanothermite reactions

Recently, we have demonstrated a new way to synthesize ferromagnetic Fe- In_2O_3 and Co- In_2O_3 nanocomposite thin films using the new thermite reactions $\text{Fe}_2\text{O}_3 + 2\text{In} = \text{In}_2\text{O}_3 + 2\text{Fe}$ [111] and $3\text{Co}_3\text{O}_4 + 8\text{In} + 4\text{In}_2\text{O}_3 + 9\text{Co}$ [112] which starts above the initiation temperature $T_{\text{in}} = 180$ °C - 190 °C with the predominant formation of the Fe, Co and In_2O_3 phases. In [113] the general strategy of the fabrication of metal oxide films has been proposed. The choice of suitable combustion precursors, containing indium nitrates as oxidizers and urea or acetyl acetone as fuel, were used for the low-temperature fabrication of In_2O_3 films. The initiation temperatures of combustion reactions, measured from DTA and DSC curves, are in the range 175 °C - 200 °C [113-115]. Our studies of the self-sustaining oxidation of In films have shown that the initiation temperature is ~ 180 °C [116]. The emergence of a strong chemical interaction between the In and O atoms above 180 °C may be the cause of rapid crystallization of amorphous In_2O_3 films within the temperature range 165-210 °C [117, 118]. The above data suggests that for the In-based nanothermites, oxidation of In and temperature crystallization of amorphous In_2O_3 films should have the same initiation temperature $T_{\text{in}} \sim 180$ °C.

It is worth noticing that all nanothermite reactions have low initiation temperatures and occur in the solid state (excluding In-based reactions). On the conceptual level, the initiation temperatures are ignored in modern models described the thin-film solid-state reactions. In contrast to this, our approach assumes the decisive role of the leading (first) phase and its initiation temperature not only in thermite reactions but also in other types of chemical reactions.

Progress in understanding and predicting the structural transformations and reactions in the solid state is limited by a lack-of-knowledge inference about the chemical interactions at nanoscale. Undoubtedly, future investigations of thin-film solid-state reactions and nanothermite reactions will discover new amazing properties of chemical interactions in solids.

4. Conclusions

The main concepts of this study are the first phase and its initiation temperature T_{in} , which describe thin-film solid-state reactions and were extended onto nanothermite reactions. The paper results prove that all Al-based nanothermite reactions have the same initiation temperature. The analysis of the initiation temperatures reported in the literature and our data has shown that the synthesis of the Al_2O_3 phase in Al/ Fe_2O_3 , Al/CuO, Al/ Co_3O_4 , Al/ MoO_3 , Al/ Bi_2O_3 , Al/NiO and Al/ Mn_2O_3 nanothermite mixtures starts at a temperature of about **510 °C**. The same initiation temperatures ~250 °C, ~450 °C, and ~180 °C also have Zr-, Mg- and In-based nanothermite reactions, respectively. Finally, these findings predict that nanothermite reactions based on other fuels (e.g., Ti and B) must have their own initiation temperatures. This approach can be widely applicable in the study of the multicomponent thin-film solid-state reactions.

Acknowledgements

I thank Zhigalov VS, Bykova LE and Matsynin AA for fruitful discussions and advice.

Compliance with ethical standards

Conflict of interest

The author has no conflict of interest related to this paper.

REFERENCES

- [1] Woodley CM, Catlow R (2008) Crystal structure prediction from first principles, *Nat Mater* 7:937- 946.
- [2] Jansen M (2015) Conceptual inorganic materials discovery – a road map, *Adv Mater* 27:3229-3242.
- [3] Tse JS, Boron charged under pressure, (2009) *Nature* 457:800-801
- [4] Desiraju GR (2013) Crystal engineering: from molecule to crystal, *J Am Chem Soc* 135:9952- 9967.

- [5] Jansen M, Schön JC (2004) Rationnal development of new materials – putting the cart before the horst, *Nat Mater* 3:838.
- [6] Walser RM, Bene' RW (1976) First phase nucleation in silicon-transition-metal planar interfaces, *Appl Phys Lett* 28:624-625.
- [7] Ronay M (1983) Reinvestigation of first phase nucleation in planar metal-Si reaction couples, *Appl Phys Lett* 42:577-579.
- [8] Grushko B, Shechtman D (1989) On the model of metastable phase formation by a diffusion process, *J Appl Phys* 67:2904-2907.
- [9] Gossele U, Tu KN (1989) "Critical thickness" of amorphous phase formation in binarydiffusion couples, *J Appl Phys* 66:2619-2626.
- [10] Ottaviani G (1979) Reviews of binary alloy formation by thin film interactions, *J Vac Sci Technol* 16:1112-1119.
- [11] Pretorius, R, Theron CC, Vantomme A, Mayer JW (1999) Compound phase formation in thin film structures, *Crit Rev Solid State Mater Sci* 24:1-62.
- [12] Poate JM, Tu KN, Meyer JW (1978) Eds: *Thin Films-Interdiffusion and Reaction*, Wiley-Interscience, New York
- [13] Colgan EG (1990) A review of thin-film aluminide formation, *Mater Sci Rep* 5:1-44.
- [14] Laurila T, Molarius J (2003) Reactive Phase Formation in Thin Film Metal/Metal and Metal/Silicon Diffusion Couples, *Crit Rev Solid State Mater Sci* 28:185-230.
- [15] Juškėnas R, Pakštas V, Sudavičius A, Kapočius V, Karpavičien V (2004) Formation of intermetallic phases during ageing of Zn electroplate on the Cu substrate, *Appl Surf Sci* 229: 402-408.
- [16] Clevenger LA, Arcot B, Ziegler W, Colgan EG, Hong QZ, d'Heurle FM Jr.; Cabral C, Gallo TA, Harper JME (1998) Interdiffusion and phase formation in Cu(Sn) alloy films, *J Appl Phys* 83: 90-99.
- [17] Boyen H-G, Indlekofer G, Gantner G, Stupp H, Cossy-Favre A, Oelhafen P (2007) Intermixing at Au-In interfaces as studied by photoelectron spectroscopy, *Phys Rev B* 51:17096-17099.
- [18] Koch Th, Siber, A, Marien J, Ziemann P (1994) Intermixing at Au-In and Pd-In interfaces at 90 K as observed by in situ Auger-electron and electron-energy-loss spectroscopy, *Phys Rev B* 49:1996 – 2000.
- [19] Fink R, Koch T, Krausch G, Marien J, Plewnia A, Runge B-U, Schatz G, Siber A, Ziemann P (1993) Formation of an ultrathin amorphous layer at In/Pd interfaces observed by local and nonlocal techniques, *Phys Rev B* 47:10048-10051.

- [20] Boyen H-G, Cossy-Favre A, Oelhafen P, Siber A, Ziemann P, Lauinger C, Moser T, Häussler P, Baumann F (1995) Low-temperature interface reactions in layered Au/Sb films: In situ investigation of the formation of an amorphous phase, *Phys Rev B* 51:791-17802.
- [21] Comrie CM, Smeets D, Pondo KJ, van der Walt C, Demeulemeester J, Knaepen W, Detavernier C, Habanyama A, Vantomme A (2012) Determination of the dominant diffusing species during nickel and palladium germanide formation, *Thin Solid Films* 526:261-268.
- [22] Chi KS, Chen LJ (2002) Dominant diffusing species in the growth of amorphous interlayer between Yb metal thin films and crystalline Si, *J Appl Phys* 92:927-931.
- [23] Adams DP (2015) Reactive multilayers fabrication by vapor deposition: a critical review, *Thin Solid Films* 576:98-128.
- [24] Weihs, T. P. In *Metallic Films for Electronic, Optical and Magnetic Applications: Structure, Processing and Properties*; Barmak, K., Coffey, K., Eds.; Woodhead Publishing Limited, 2014; Chapter 5, pp 160-243.
- [25] Rossi C, Zhang K, Esteve D, Alphonse P, Tailhades P, Vahlas C (2007) Nanoenergetic Materials for MEMS: A Review, *J Microelectromech Syst* 16:919-931.
- [26] Mukasyan AS, Rogachev AS, Reddy Aruna ST (2015) Combustion synthesis in nanostructured reactive systems, *Adv Powder Technol* 26:954-976.
- [27] Dreizin EL (2009) Metal-based reactive nanomaterials. *Prog Energy Combust Sci* 35:141-167.
- [28] Wang LL, Munir ZA, Maximov YM (1993) Thermite reactions: their utilization in the synthesis and processing of materials, *J Mater Sci* 28:3693-3708.
- [29] Yang Y, Yan D-r, Dong Y-c, Chen X-g, Wang L, Chu Z.-h, Zhang J-x, He J-n (2013) Influence of oxides addition on the reaction of Fe₂O₃-Al composite powders in plasma flame, *J Alloy Compd* 579:1-6.
- [30] Babakhani A, Zahabi E, Mehrabani HY (2012) Fabrication of Fe/Al₂O₃ composite foam via combination of combustion synthesis and spark plasma sintering techniques, *J Alloys Compd* 514:20-24.
- [31] Myagkov VG, Bykova LE, Bondarenko GN, Zhigalov VS, Pol'skii AI, Myagkov FV (2000) Solid-phase reactions self-propagating high-temperature synthesis, and order-disorder phase transition in thin films, *JETP Letters* 71:183-186.
- [32] Myagkov VG, Zhigalov VS, Bykova LE, Bondarenko GN (2006) Solid-state synthesis and phase transformations in Ni/Fe films: structural and magnetic studies, *J Magn Magn Mater* 305:534-545.
- [33] Myagkov VG, Bykova LE, Zharkov SM, Bondarenko GN (2008) Formation of NiAl shape memory alloy thin films by solid-state reaction, *Solid State Phenomena* 138:377-384.

- [34] Myagkov VG, Mikhlin YuL, Bykova LE, Bondarenko GV, Bondarenko GN (2010) Long-Range Nature of Chemical Interaction in Solid-Phase Reactions: Formation of Martensite Phases of an Au–Cd Alloy in Cd/Fe/Au Film Systems, *Dokl Phys Chem* 431:52-56.
- [35] Myagkov VG, Bykova LE, Bondarenko GN (1999) Multiple self-propagating high-temperature synthesis and solid-phase reactions in thin films, *JETP* 88:963-967.
- [36] Myagkov VG, Bykova LE, Bondarenko GN (2003) Solid-State Synthesis and Martensitic Transformations in Thin Films, *Dokl Physics* 48:30 – 33.
- [37] Myagkov VG, Zhigalov VS, Matsynin AA, Bykova LE, Bondarenko GV, Bondarenko GN, Patrino GS, Velikanov DA (2012) Phase transformations in the Mn-Ge system and in $\text{Ge}_x\text{Mn}_{1-x}$ diluted semiconductors, *JETP Letters* 96:40-43.
- [38] Myagkov VG, Zhigalov VS, Matsynin AA, Bykova LE, Mikhlin YuL, Bondarenko GN, Patrino GS, Yurkin GYu (2014) Formation of ferromagnetic germanides by solid-state reactions in 20Ge/80Mn films, *Thin Solid Films* 552:86 – 91.
- [39] Fritz GM, Spey SJ Jr, Grapes MD, Weihs TP (2013) Thresholds for igniting exothermic reactions in Al/Ni multilayers using pulses of electrical, mechanical, and thermal energy, *J Appl Phys* 113:014901-014901-10.
- [40] Tillotson TM, Gash AE, Simpson RL, Hrubesh LW, Satcher JH Jr, Poco JF (2001) Nanostructured energetic materials using sol–gel methodologies, *J Non-Crystalline Solids* 285:338-345.
- [41] Shin M-S, Kim J-K, Kim J-W, Moraes CAM, Kim H-S, Koo K-K (2012) Reaction characteristics of Al/Fe₂O₃ nanocomposites, *J Indus Eng Chemistry* 18:1768-1773.
- [42] Chen JL, Hng HH, Lee YW, Du SW, Thadhani NN (2010) Kinetic study of thermal- and impact-initiated reactions in Al–Fe₂O₃ nanothermite, *Combust. Flame* 157:2241-2249.
- [43] Kim SH, Zachariah MR (2004) Enhancing the Rate of Energy Release from NanoEnergetic Materials by Electrostatically Enhanced Assembly, *Adv Mater* 16:1821-1825.
- [44] Zhang W, Yin B, Shen R, Ye J, Thomas JA, Chao Y (2013) Significantly Enhanced Energy Output from 3D Ordered Macroporous Structured Fe₂O₃/Al Nanothermite Film, *ACS Appl Mater Interfaces* 5:239-242.
- [45] Myagkov VG, Polyakova KP, Bondarenko GN, Polyakov VV (2003) Granular Fe–Al₂O₃ films prepared by self-propagating high temperature synthesis, *J Magn Magn Mater* 258-259:358-360.
- [46] Guo-Qiang Z, Wen-Chao Z, Xing X, Rui-Qi S, Ji-Ping D, Ying-Hua YE (2015) Preparation of Porous Core/Shell Structure Fe₂O₃/Al Nanothermite Membrane by Template Method, *J Inorg Mater* 30:610-614.

- [47] Sui H, Atashin S, Wen JZ (2016) Thermo-chemical and energetic properties of layered nano-thermite composites, *Thermochim. Acta* 642:17-24.
- [48] Ke X, Zhou X, Hao G, Xiao L, Liu J, Jiang W (2017) Rapid fabrication of superhydrophobic Al/Fe₂O₃ nanothermite film with excellent energy-release characteristics and long-term storage stability, *Appl Surf Sci* 407:137–144.
- [49] Guo-Qiang Z, Wen-Chao Z, Xing X, Rui-Qi S, Ji-Ping D, Ying-Hua Y (2015) Preparation of Porous Core/Shell Structure Fe₂O₃/Al Nanothermite Membrane by Template Method, *J Inorg Mater* 30:610-614.
- [50] Qin L, Yan N, Li J, Hao H, Zhao F, Feng H (2017) Enhanced energy performance from core-shell structured Al@Fe₂O₃ nanothermite fabricated by atomic layer deposition, *RSC Adv* 7:7188-7197.
- [51] Yan N, Qin L, Hao H, Hui L, Zhao F, Feng H (2017) Iron oxide/aluminum/graphene energetic nanocomposites synthesized by atomic layer deposition: Enhanced energy release and reduced electrostatic ignition hazard, *Appl Surf Sci* 408:51-59.
- [52] Zhang T, Ma Z, Li G, Wang Z, Zhao B, Luo Y (2016) Electrostatic interactions for directed assembly of high performance nanostructured energetic materials of Al/Fe₂O₃/multi-walled carbon nanotube (MWCNT), *J Solid State Chem* 237:394–403.
- [53] Zhang T, Wang Z, Li G, Luo Y (2015) Tuning the reactivity of Al/Fe₂O₃ nanoenergetic materials via an approach combining soft template self-assembly with sol-gel process, *J Solid State Chem* 230:1-7.
- [54] Zhou X, Ying Zhu Y, Ke X, Zhang K (2019) Exploring the solid-state interfacial reaction of Al/Fe₂O₃ nanothermites by thermal analysis, *J Mater Sci* (2019) 54:4115–4123.
- [55] Yang Y, Xu D, Zhang K (2012) Effect of nanostructures on the exothermic reaction and ignition of Al/CuO_x based energetic materials, *J Mater Sci* 47:1296-1305.
- [56] Kwon J, Ducéré JM, Alphonse P, Bahrami M, Petrantonni M, Veyan J-F, Tenailleau C, Estève A, Rossi C, Chabal YJ (2013) Interfacial Chemistry in Al/CuO Reactive Nanomaterial and Its Role in Exothermic Reaction, *ACS Appl Mater Interfaces* 5: 605-613.
- [57] Petrantonni M, Rossi C, Salvagnac L, Conédéra V, Estève A, Tenailleau C, Alphonse P, Chabalet YJ (2010) Multilayered Al/CuO thermite formation by reactive magnetron sputtering: Nano versus micro, *J Appl Phys* 108:084323-0843.
- [58] Kim DK, Bae JH, Kang MK, Kim HJ (2011) Analysis on thermite reactions of CuO nanowires and nanopowders coated with Al, *Curr Appl Phys* 11:1067-1070.
- [59] Chiang Y-C, Wu M-H (2017) Assembly and reaction characterization of a novel thermite consisting aluminum nanoparticles and CuO nanowires, *Proc Combust Inst* 6:4201-4208.

- [60] Sui H, LeSergent L, Wen JZ (2017) Diversity in Addressing Reaction Mechanisms of Nano-Thermite Composites with a Layer by Layer Structure, *Adv Eng Mater* 20:1700822-1 - 1700822-11.
- [61] Yin Y, Li X, Shu Y, Guo X, Zhu Y, Huang X, Bao H, Xu K (2017) Highly-reactive Al/CuO nanoenergetic materials with a tubular structure, *Mater Design* 117:104-110.
- [62] Abdallah I, Zapata J, Lahiner G, Warot-Fonrose B, Cure J, Chabal Y, Esteve A, Rossi C (2018) Structure and Chemical Characterization at the Atomic Level of Reactions in Al/CuO Multilayers, *ACS Appl Energy Mater* 1:1762-1770.
- [63] Dai J, Wang F, Ru C, Xu J, Wang C, Zhang W, Ye Y, Shen R (2018) Ammonium Perchlorate as an Effective Additive for Enhancing the Combustion and Propulsion Performance of Al/CuO Nanothermites, *J Phys Chem C* 122:10240-10247.
- [64] Shen J, Qiao Z, Zhang K, Wang J, Li R, Xu H, Yang G, Nie F (2014) Effects of nano-Ag on the combustion process of Al-CuO metastable intermolecular composite, *Appl Therm Eng* 62:732-737.
- [65] Zhou X, Wang Y, Cheng Z, Ke X, Jiang W (2017) Facile preparation and energetic characteristics of core-shell Al/CuO metastable intermolecular composite thin film on a silicon substrate, *Chem Eng J* 328:585-590.
- [66] Shen J, Qiao Z, Wang J, Yang G, Chen J, Li Z, Liao X, Wang H, Zachariah MR (2018) Reaction mechanism of Al-CuO nanothermites with addition of multilayer graphene, *Thermochim Acta* 666:60-65.
- [67] Glavier L, Taton G, Ducéré J-M, Baijot V, Pinon S, Calais T, Estève A, Rouhani MD, Rossi C (2015) Nanoenergetics as pressure generator for nontoxic impact primers: Comparison of Al/Bi₂O₃, Al/CuO, Al/MoO₃ nanothermites and Al/PTFE, *Combust Flame* 162:1813-1820.
- [68] Zhu Y, Zhou X, Xu J, Ma X, Ye Y, Yang G, Zhang K (2018) In situ preparation of explosive embedded CuO/Al/CL20 nanoenergetic composite with enhanced reactivity, *Chem Eng J* 354:885-895.
- [69] Pantoya ML, Granier JJ (2005) Combustion Behavior of Highly Energetic Thermites: Nano versus Micron Composites, *Propel Expl Pyrotech* 30:53-62.
- [70] Umbrajkar SM, Chen C-M., Schoenitz M, Dreizin EL (2008) On problems of isoconversion data processing for reactions in Al-rich Al-MoO₃ thermites, *Thermochim Acta* 477:1-6.
- [71] Xu J, Tai Y, Ru C, Dai J, Ye Y, Shen R, Zhu P (2017) Tuning the Ignition Performance of a Microchip Initiator by Integrating Various Al/MoO₃ Reactive Multilayer Films on a Semiconductor Bridge, *ACS Appl Mater Interfaces* 9:5580-5589.
- [72] Hu X, Xiao L, Jian X, Zhou W (2018) Integration of nano-Al with one-step synthesis of MoO₃ nanobelts to realize high exothermic nanothermite, *Sci Eng Compos Mater* 25:579-585

- [73] Seo H-S, Kim J-K, Kim J-W, Kim H-S, Koo K-K (2014) Thermal behavior of Al/MoO₃ xerogel nanocomposites, *J Ind Eng Chem* 20:189–193.
- [74] Zakiyyan N, Wang A, Thiruvengadathan RR, Staley C, Mathai J, Gangopadhyay K, Maschmann MR (2018) Combustion of aluminum nanoparticles and exfoliated 2D molybdenum trioxide composites, *Combust Flame* 187:1-10.
- [75] Puszynski JA, Bulian CJ, Swiatkiewicz JJ (2007) Processing and Ignition Characteristics of Aluminum-Bismuth Trioxide Nanothermite System, *J Propul Power* 23:698-706.
- [76] Patel VK, Ganguli A, Kant RR, Bhattacharya SS (2015) Micropatterning of nanoenergetic films of Bi₂O₃/Al for pyrotechnics, *RSC Adv* 5:14967-14973.
- [77] Dai J, Xu J, Wang F, Tai Y, Shen Y, Shen R, Ye Y (2018) Facile formation of nitrocellulose-coated Al/Bi₂O₃ nanothermites with excellent energy output and improved electrostatic discharge safety, *Mater Design* 143:93-103.
- [78] Hobosyan MA, Yolchinyan SA, Martirosyan KS (2016) A novel nano-energetic system based on bismuth hydroxide, *RSC Adv* 6:66564-66570.
- [79] Xu D, Yang Y, Cheng H, Li YY, Zhang K (2012) Integration of nano-Al with Co₃O₄ nanorods to realize high-exothermic core-shell nanoenergetic materials on a silicon substrate, *Combust Flame* 159:2202-2209.
- [80] Yu C, Zhang W, Gao Y, Ni D, Ye J, Zhu C, Ma K (2018) The super-hydrophobic thermite film of the Co₃O₄/Al core/shell nanowires for an underwater ignition with a favorable aging-resistance, *Chem Eng J* 338:99-106
- [81] Zheng Z, Zhang W, Yu C, Zheng G, Ma K, Qin Z, Ye J, Chao Y (2018) Integration of the 3DOM Al/Co₃O₄ nanothermite film with a semiconductor bridge to realize a high output micro-energetic igniter, *RSC Adv* 8:2552-2560.
- [82] Xiao F, Li J, Zhou X, Yang R (2018) Preparation of mechanically activated aluminum rich Al-Co₃O₄ powders and their thermal properties and reactivity with water steam at high temperature, *Combust Sci Technol* 190:1935-1949.
- [83] Patel VK, Saurav JR, Gangopadhyay K, Gangopadhyay S, Bhattacharya S (2015) Combustion characterization and modeling of novel nanoenergetic composites of Co₃O₄/nAl, *RSC Adv* 5:21471-21479.
- [84] Myagkov VG, Bykova LE, Zhigalov VS, Matsynin AA, Volochaev MN, Tambasov IA, Mikhlin YuL, Bondarenko GN (2017) Thermite synthesis, structural and magnetic properties of Co-Al₂O₃ nanocomposite films, *J Alloys Compd* 724:820-826.
- [85] Volochaev MN, Komogortsev SV, Myagkov VG, Bykova LE, Zhigalov VS, Shestakov NP, Velikanov DA, Smolyakov DA, Luk'yanenko AV, Rachek VB, Loginov YY, Tambasov IA,

- Matsynin AA (2018) Structural and magnetic characteristics of nanogranular Co–Al₂O₃ single- and multilayer films formed by the solid-state synthesis, *Phys solid state* 60:1425-1431.
- [86] Wen JZ, Ringuette S, Bohlouli-Zanjani G, Hu A, Nguyen NH, Persic J, Petre CF, Zhou YN (2013) Characterization of thermochemical properties of Al nanoparticles and NiO nanowire composites, *Nanoscale Res Lett* 8:184-1-184-9.
- [87] Bohlouli-Zanjania G, Wen JZ, Hu A, Persic J, Ringuette S, Zhou YN (2013) Thermochemical characterization of a Al nanoparticle and NiO nanowire composite modified by Cu powder, *Thermochim Acta* 572:51-58.
- [88] Yu C, Zhang W, Shen R, Xu X, Cheng J, Ye J, Qin Z, Chao Y (2016) 3D ordered macroporous NiO/Al nanothermite film with significantly improved higher heat output, lower ignition temperature and less gas production, *Mater. Design* 110:304-310.
- [89] Zhang D, Li X (2015) Fabrication and Kinetics Study of Nano-Al/NiO Thermite Film by Electrophoretic Deposition, *J Phys Chem A* 119:4688-4694.
- [90] Zheng G, Zhang W, Shen R, Ye J, Qin Z, Chao Y (2016) Three-dimensionally Ordered Macroporous Structure Enabled Nanothermite Membrane of Mn₂O₃/Al, *Sci Rep* 6:22588; doi: 10.1038/srep22588.
- [91] Yang Y, Zhang Z-C, Wang P-P, Zhang J-C, Nosheen F, Zhuang J, Wang X (2013) Hierarchical MnO₂/SnO₂ Heterostructures for a Novel Free-Standing Ternary Thermite Membrane, *Inorg Chem* 52:9449-9455.
- [92] Kearns M (2004) Development and applications of ultrafine aluminium powders, *Mater Sci Eng A* 375–377:20-126
- [93] Jones DEG, Brousseau P, Fouchard RC, Turcotte AM, Kwok QSM (2000) Thermal Characterization of Passivated Nanometer Size Aluminium Powders, *J Therm Anal Cal* 2000 61:805-818.
- [94] Dreizin EL, Schoenitz M (2015) Correlating ignition mechanisms of aluminum-based reactive materials with thermoanalytical measurements, *Prog Energy Combust Sci* 50:81-105.
- [95] Zha M, Lv X, Ma Z, Zhang L, Zhao F, Xu S, Xu H (2015) Effect of Particle Size on Reactivity and Combustion Characteristics of Aluminum Nanoparticles, *Combust Sci Technol* 187:1036-1043.
- [96] Noor F, Zhang H, Korakianitisac T, Wen D (2013) Oxidation and ignition of aluminum nanomaterials, *Phys Chem Chem Phys* 15:20176-20188.
- [97] Saceleanu F, Atashin S, Wen JZ (2017) Investigation of the effects of phase transformations in micro and nano aluminum powders on kinetics of oxidation using thermogravimetric analysis, *Phys Chem Chem Phys* 19:18996-19009.

- [98] Wang F, Wu Z, Shanguan X, Sun Y, Feng J, Li Z, Chen L, Zuo S, Zhuo R, Yan P (2017) Preparation of mono-dispersed, high energy release, core/shell structure Al nanopowders and their application in HTPB propellant as combustion enhancers, *Sci Rep* 7:5228, DOI:10.1038/s41598-017-05599-0.
- [99] Coulet M-V, Rufino B, Esposito P-H, Neisius T, Isnard O, Denoyel R (2015) Oxidation Mechanism of Aluminum Nanopowders, *J Phys Chem C* 119:25063-25070.
- [100] Vorozhtsov AB, Lerner M, Rodkevich N, Nie H, Abraham A, Schoenitz M, Dreizin EL (2016) Oxidation of nano-sized aluminum powders, *Thermochim Acta* 636:48–56.
- [101] Chen Y, Zhang W, Yu C, Ni D, Ma K, Ye J (2018) Controllable synthesis of NiCo₂O₄/Al core-shell nanowires thermite film with excellent heat release and short ignition time, *Mater Design* 155:396-403.
- [102] Shi L, Zhang W, Cheng J, Yu C, Shen R, Ye J, Qin Z, Chao Y (2016) A high energy output and low onset temperature nanothermite based on three-dimensional ordered macroporous nano-NiFe₂O₄, *RSC Adv* 6:93330-93334.
- [103] Myagkov VG, Zhigalov VS, Bykova LE, Zharkov SM, Matsynin AA, Volochaev MN, Tambasov IA, Bondarenko GN (2016) Thermite synthesis and characterization of Co-ZrO₂ ferromagnetic nanocomposite thin films, *J Alloys Compd* 665:197–203.
- [104] Myagkov VG, Bykova LE, Bayukov OA, Zhigalov VS, Tambasov IA, Zharkov SM, Matsynin AA, Bondarenko GN (2015) Solid state synthesis and characterization of Fe–ZrO₂ ferromagnetic nanocomposite thin films, *J Alloys Compd* 636:223-228.
- [105] Mily EJ, Oni A, LeBeau JM, Liu Y, Brown-Shaklee HJ, Ihlefeld JF, Maria J-P (2014) The role of terminal oxide structure and properties in nanothermite reactions, *Thin Solid Films* 562:405-410.
- [106] Kim J-S, Lee D-H, Kang S, Bae D-S, Park H-Y, Na M-K (2009) Synthesis and microstructure of zirconia nanopowders by glycothermal processing, *Trans Nonferrous Met Soc China* 19:s88-s91.
- [107] Zhou X, Xu D, Zhang Q, Lu J, Zhang K (2013) Facile Green In Situ Synthesis of Mg/CuO Core/Shell Nanoenergetic Arrays with a Superior Heat-Release Property and Long-Term Storage Stability, *ACS Appl Mater Interfaces* 5:7641–7646.
- [108] Zhou X, Xu D, Zhang Q, Lu J, Zhang K (2015) CuO/Mg/fluorocarbon sandwich-structure superhydrophobic nanoenergetic composite with anti-humidity property, *Chem Eng J* 266:163-170.
- [109] Hosseini SG, Sheikhpour A, Keshavarz MH, Tavangar S (2016) The effect of metal oxide particle size on the thermal behavior and ignition kinetic of Mg–CuO thermite mixture, *Thermochim Acta* 626:1-8.

- [110] Chunmiao Y, Lifu Y, Chang L, Gang L, Shengjun Z (2013) Thermal analysis of magnesium reactions with nitrogen/oxygen gas mixture, *J Hazard Mater* 260:707-714.
- [111] Myagkov VG, Tambasov IA, Bayukov OA, Zhigalov VS, Bykova LE, Mikhlin YL, Volochaev MN, Bondarenko GN (2014) Solid State Synthesis and Characterization of ferromagnetic nanocomposite Fe-In₂O₃ thin films, *J Alloys Compd* 612:189-194.
- [112] Bykova LE, Zhigalov VS, Myagkov VG, Volochaev MN, Matsynin AA, Bondarenko GN, Patrino GS (2018) Co-In₂O₃ Nanocomposite films: synthesis and structural and magnetic properties, *Phys solid state* 60:2072-2077.
- [113] Kim M-G, Kanatzidis MG, Facchetti A, Marks TJ (2011) Low-temperature fabrication of high-performance metal oxide thin-film electronics via combustion processing, *Nat Mater* 10:382-388.
- [114] Sanchez-Rodriguez D, Farjas J, Roura P, Ricart S, Mestres N, Obradors X, Puig T (2013) Thermal Analysis for Low Temperature Synthesis of Oxide Thin Films from Chemical Solutions, *J Phys Chem C* 117:20133-20138.
- [115] Yu X, Zhou N, Smith J, Lin H, Stallings K, Yu J, Marks TJ, Facchetti A (2013) Synergistic Approach to High-Performance Oxide Thin Film Transistors Using a Bilayer Channel Architecture, *ASC Appl Mater Interfaces* 5:7983-7988.
- [116] Tambasov IA, Myagkov VG, Ivanenko AA, Nemtsev IV, Bykova LE, Bondarenko GN, Mikhlin YL, Maksimov IA, Ivanov VV, Balashov SV, Karpenko DS (2013) Structural and Optical Properties of Thin In₂O₃ Films Produced by Autowave Oxidation, *Semiconductors* 47:569-573.
- [117] Thilakan P, Kumar J (1998) Oxidation dependent crystallization behaviour of IO and ITO thin films deposited by reactive thermal deposition technique, *Mater Sci Eng B* 55:195-200 (115)
- [118] Adurodija FO, Semple L, Brüning RJ (2006) Crystallization process and electro-optical properties of In₂O₃ and ITO thin films. *J Mater Sci* 41:7096-7102.

Figure 1. The schematic illustration of the initiation temperature $T_{in} \sim 510 \text{ }^\circ\text{C}$ for the Al-based nanothermite reactions with Fe_2O_3 , Co_3O_4 , NiO , MnO_2 , Bi_2O_3 , CuO , MoO_3 oxidizers and the oxidation of Al nanomaterials. The initiation temperature $T_{in} \sim 510 \text{ }^\circ\text{C}$ is characteristic of the leading Al_2O_3 phase, which has a high negative enthalpy of formation ($\Delta H_f = -1676 \text{ kJ/mol}$) and is the driving force of all the Al-based nanothermite reactions.

Table 1. Summary of Al-based nanothermite reactions with Fe_2O_3 oxidizer and with an associated record of the initiation temperatures.

Table 2. Summary of Al-based nanothermite reactions with CuO oxidizer and with an associated record of the initiation temperatures.

Table 3. Summary of Al-based nanothermite reactions with Bi_2O_3 , MoO_3 oxidizers and with an associated record of the initiation temperatures.

Table 4. Summary of Al-based nanothermite reactions with Co_3O_4 , NiO , MnO_2 , oxidizers and with an associated record of the initiation temperatures.

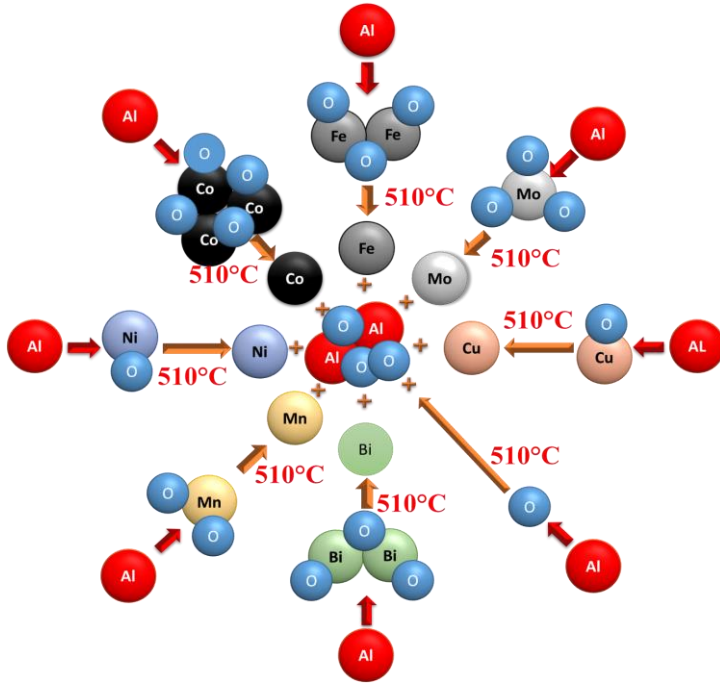


Figure 1. The schematic illustration of the initiation temperature $T_{in} \sim 510 \text{ }^{\circ}\text{C}$ for the Al-based nanothermite reactions with Fe_2O_3 , Co_3O_4 , NiO , MnO_2 , Bi_2O_3 , CuO , MoO_3 oxidizers and the oxidation of Al nanomaterials. The initiation temperature $T_{in} \sim 510 \text{ }^{\circ}\text{C}$ is characteristic of the leading Al_2O_3 phase, which has a high negative enthalpy of formation ($\Delta H_f = -1676 \text{ kJ/mol}$) and is the driving force of all the Al-based nanothermite reactions.

Table 1. Summary of Al-based nanothermite reactions with Fe₂O₃ oxidizer and with an associated record of the initiation temperatures.

| Nanothermite Systems | Initiation Temperature T _{in} (°C) | Techniques | Temperature Rate η (K/min.) | Exothermic Peak Temperature (°C) | Samples | Refs. |
|-----------------------------------|---|------------------------------|-----------------------------|----------------------------------|--|-------|
| Al/Fe ₂ O ₃ | ~ 490 | DSC | 10 | ~ 530 | Fe ₂ O ₃ /Al xerogel nanocomposites | [40] |
| Al/Fe ₂ O ₃ | ~ 530 | TGA/DSC | 10 | ~ 550 | Fe ₂ O ₃ /Al xerogel nanocomposites | [41] |
| Al/Fe ₂ O ₃ | ~ 510 | DSC | 10 | 588 | Fe ₂ O ₃ nanotubes, Al nanocomposites | [42] |
| Al/Fe ₂ O ₃ | ~ 520 | DSC | 10 | ~ 545 | Fe ₂ O ₃ nanoporous particles, Al powder | [43] |
| Al/Fe ₂ O ₃ | ~ 520 | DSC | 20 | 548 | Fe ₂ O ₃ /Al nanothermite membranes. | [44] |
| Al/Fe ₂ O ₃ | ~ 530 | Magnetization vs temperature | > 10 | | Fe ₂ O ₃ /Al bilayers. | [45] |
| Al/Fe ₂ O ₃ | ~ 525 | TGA/DSC | 8-30 | ~ 590 | Fe ₂ O ₃ /Al nanothermite membranes | [46] |
| Al/Fe ₂ O ₃ | 507-508 | TGA/DSC | 10 | ~ 590 | Fe ₂ O ₃ , Al nanoparticles | [47] |
| Al/Fe ₂ O ₃ | ~ 520 | TGA/DTA | 20 | ~ 620 | Al/Fe ₂ O ₃ nanothermite film | [48] |
| Al/Fe ₂ O ₃ | ~ 490 | TGA/DTA | 10 | ~ 570 | Porous Core/Shell Structure Fe ₂ O ₃ /Al | [49] |
| Al/Fe ₂ O ₃ | ~ 490 | DSC | 10 | ~ 570 | core-shell structured Al@Fe ₂ O ₃ nanothermite | [50] |
| Al/Fe ₂ O ₃ | ~ 500 | DSC | 20 | ~ 550 | Al@Fe ₂ O ₃ nanocomposites | [51] |
| Al/Fe ₂ O ₃ | ~ 500 | TGA/DSC | 10 | ~ 590 | Al/Fe ₂ O ₃ /MWCNT nanostructured energetic materials | [52] |
| Al/Fe ₂ O ₃ | ~ 480 | DSC | 20 | ~ 560 | nanostructured energetic materials sol-gel-Al/Fe ₂ O ₃ | [53] |
| Al/Fe ₂ O ₃ | 504-525 | DSC/TG | 5 | 546-569 | n-Al/n-Fe ₂ O ₃ nanothermite | [54] |

Table 2. Summary of Al-based nanothermite reactions with CuO oxidizer and with an associated record of the initiation temperatures.

| Nanothermite Systems | Initiation Temperature T_{in} (°C) | Techniques | Temperature Rate η (K/min.) | Exothermic Peak Temperature (°C) | Samples | Refs. |
|----------------------|--------------------------------------|------------|----------------------------------|----------------------------------|---|-------|
| Al/CuO | ~ 520 | DTA/DSC | 15/5 | 580/560 | CuO nanowires, Al films. | [55] |
| Al/CuO | 515 | DSC | 10 | ~ 530 | Al/CuO bilayers | [56] |
| Al/CuO | ~ 520 | DTA/DSC | 5 | ~ 560 | Al/CuO multilayers | [57] |
| Al/CuO | ~ 500 | TG/DSC | 15 | ~ 540 | CuO nanowires coated with deposited nano-Al | [58] |
| Al/CuO | ~ 520 | DTA/DSC | 10 | ~ 566 | CuO nanowires, Al nanoparticles | [59] |
| Al/CuO | ~ 500 | TGA/DSC | 10 | ~ 560 | Al, CuO nanoparticles | [60] |
| Al/CuO | ~ 500 | DSC/TG | 10 | ~ 620 | nanoAl, CuO nano-array | [61] |
| Al/CuO | ~ 500 | DSC | 10 | ~ 550 | CuO/Al multilayers | [62] |
| Al/CuO | ~ 520 | DSC | 5 | ~ 540 | Al, CuO nanoparticles | [63] |
| Al/CuO | ~ 500 | DSC | 10 | ~ 560 | Al, CuO nanoparticles | [64] |
| Al/CuO | ~ 520 | DSC | 5 | ~ 560 | Al/CuO nanoparticles core-shell structures | [65] |
| Al/CuO | ~ 530 | DG/DSC | 10 | ~ 590 | Al, CuO nanoparticles | [66] |
| Al/CuO | ~ 480 | DSC | 10 | ~ 550 | Al, CuO nanoparticles | [67] |
| Al/CuO | ~ 480 | DSC | 10 | ~ 550 | Al/CuO core/shell arrays | [68] |

Table 3. Summary of Al-based nanothermite reactions with Bi₂O₃, MoO₃ oxidizers and with an associated record of the initiation temperatures.

| Nanothermite Systems | Initiation Temperature T _{in} (°C) | Techniques | Temperature Rate η (K/min.) | Exothermic Peak Temperature (°C) | Samples | Refs. |
|-----------------------------------|---|------------|-----------------------------|----------------------------------|--|-------|
| Al/MoO ₃ | 476 | DTS | 10 | ~ 500 | MoO ₃ nanoparticles, Al micro particles | [69] |
| Al/MoO ₃ | ~ 500 | DTS | 10 | ~ 550 | Al/MoO ₃ nanocomposites | [70] |
| Al/MoO ₃ | ~ 520 | DSC | 20 | ~ 560-590 | Reactive multilayer films | [71] |
| Al/MoO ₃ | ~ 475-515 | DTA/DSC | | ~ 550 | nano-Al, MoO ₃ nanobelts | [72] |
| Al/MoO ₃ | ~ 520 | TG/DSC | 10 | ~ 560 | Al/MoO ₃ xerogel nanocomposite | [73] |
| Al/MoO ₃ | ~ 440 | TGA/DSC | 20 | ~ 520 | (2D) molybdenum trioxide, Al nanoparticles | [74] |
| Al/MoO ₃ | ~ 480 | DSC | 10 | ~ 550 | Al, MoO ₃ nanoparticles | [67] |
| | | | | | | |
| Al/Bi ₂ O ₃ | ~ 520 | DTS | 10 | ~ 550 | Al, Bi ₂ O ₃ nanopowders | [75] |
| Al/Bi ₂ O ₃ | ~ 510 | TG/DTS | 10 | ~ 572/589 | Al, Bi ₂ O ₃ nanofilms | [76] |
| Al/Bi ₂ O ₃ | ~ 480 | DSC | 20 | 591 | Al, Bi ₂ O ₃ nanoparticles | [77] |
| Al/Bi(OH) ₃ | ~ 520 | DSC | 20 | 603 | Al-Bi(OH) ₃ nanothermite | [78] |
| Al/Bi ₂ O ₃ | ~ 480 | DSC | 10 | ~ 550 | Al, Bi ₂ O ₃ nanoparticles | [67] |

Table 4. Summary of Al-based nanothermite reactions with Co_3O_4 , NiO, MnO_2 , oxidizers and with an associated record of the initiation temperatures.

| Nanothermite Systems | Initiation Temperature T_{in} ($^{\circ}\text{C}$) | Techniques | Temperature Rate η (K/min.) | Exothermic Peak Temperature ($^{\circ}\text{C}$) | Samples | Refs. |
|---------------------------------------|--|---|----------------------------------|--|---|---------|
| Al/ Co_3O_4 | ~ 520 | DTA/TGA | 10 | 574/569 | Co_3O_4 nanowires, nano-Al | [79] |
| Al/ Co_3O_4 | ~ 551 | DSC | 10 | ~ 600 | Co_3O_4 /Al core/shell nanowires | [80] |
| Al/ Co_3O_4 | ~ 500 | DSC | 10-30 | ~ 560-590 | Al/ Co_3O_4 nanothermites film | [81] |
| Al/ Co_3O_4 | ~ 500 | DSC | 10 | ~ 560-590 | the Co_3O_4 particles were embedded in the aluminum particles | [82] |
| Al/ Co_3O_4 | ~ 535 | TG-DSC | 10 | ~ 605 | Co_3O_4 /nanoAl | [83] |
| Al/ Co_3O_4 | ~ 510 | Magnetization and electrical resistance as a function temperature | ~ 4 | | Co_3O_4 /Al nanofilms | [84-85] |
| | | | | | | |
| Al/NiO | ~ 475-515 | DTA/DSC | 10 | ~ 550 | NiO nanowires, Al nanoparticles | [86] |
| Al/NiO | ~ 490 | DSC | 10 | ~ 549 | NiO nanowires, Al nanoparticles | [87] |
| Al/NiO | ~ 460 | DSC | 20 | ~ 530-565 | Three-dimensionally ordered macroporous NiO/Al nanothermite film. | [88] |
| Al/NiO | ~ 520 | DSC | 20 | ~ 590 | Nano-Al/NiO thermite films | [89] |
| Al/NiO | ~ 516 | DGA/DSC | 10 | ~ 535 | Al/NiO thermite Film | [60] |
| | | | | | | |
| Al/ Mn_2O_3 | 474-518 | DSC | 20 | 563-599 | Mn_2O_3 macroporous skeleton, Al films | [90] |
| MnO_2 / SnO_2 /n-Al | ~520 | DSC | 20 | 600 | MnO_2 / SnO_2 /n-Al ternary thermite membrane | [91] |